RSC Advances

Ageing behavior of the silicone dielectric elastomers in simulated marine environment

Journal:	*RSC Advances*
Manuscript ID	Draft
Article Type:	Paper
Date Submitted by the Author:	n/a
Complete List of Authors:	Bele, Adrian; "Petru Poni" Institute of Macromolecular Chemistry, Stiubianu, George Theodor; "Petru Poni" Inatitute of Macromolecular Chemistry, Inorganic Polymers Vlad, Stelian; "Petru Poni" Institute of Macromolecular Chemistry, Tugui, Codrin; "Petru Poni" Institute of Macromolecular Chemistry, Inorganic Polymers Varganici, Cristian-Dragos; "Petru Poni" Institute of Macromolecular Chemistry, Centre of Advanced Research in Bionanoconjugates and Biopolymers Matricala, Ana-Lavinia; Petru Poni Institute of Macromolecular Chemistry, Timpu, Daniel; "Petru Poni" Institute of Macromolecular Chemistry, Cazacu, Maria; "Petru Poni" Institute of Macromolecular Chemistry, Inoeganic Polymers
Subject area & keyword:	Composites < Materials

Ageing behavior of the silicone dielectric elastomers in simulated marine environment

A. Bele[a], G. Stiubianu[a], S. Vlad[a], C. Tugui[a], C.D. Varganici[a], L. Matricala[a], D. Timpu[a], M. Cazacu[a]

[a] *"Petru Poni" Institute of Macromolecular Chemistry, Aleea Gr. Ghica Voda 41A, 700487 Iasi, Romania*

Abstract

A series of silicone-barium titanate composites (multiple specimens of each sample) designed as dielectric elastomeric films were immersed in artificial sea water (ASW) in pseudo-dynamic conditions. While part of specimens were extracted after one half year and subsequently subjected to UV irradiation for 500 h (protocol A), the rest were kept in the saline environment until one year (protocol B). The changes occurred in the structure and morphology as well as in mechanical and dielectric properties were assessed by comparing the obtained results to those of the original samples. The thermal transitions were identified from the differential scanning calorimetry data and based on them, the crystallinity degrees of the samples were evaluated in each of the three stages. The tensile toughness, the amount of energy per volume unit that the material can absorb until failure, was estimated as area under tensile stress-strain curves. The toughness at 100 % elongation was determined on the basis of cyclic stress-strain curves of the original samples as an indirect measure of the energy that the elastic material could release when force that acted on it is removed, like in a harvesting energy system. As a general trend, it can be said that the samples based on the lowest molecular mass polymer (Mn = 40 000) and consequently the highest crosslinking degree show the most convenient characteristics but these are the most affected by the ageing process.

Keywords: Polymer-matrix composites, Environmental degradation, Mechanical properties, Electrical properties, Silicones

1. Introduction

Silicone rubber is a well-known dielectric elastomer used in electromechanical devices such as actuators or devices for harvesting energy from various natural sources, i.e., human body motion, wind, or ocean waves.[1] Depending on the working and environment conditions, an evaluation of maintenance periods and total lifetime is necessary because degradation processes appear when material is used for long term in outdoor conditions. Therefore, it is important to identify the principal factors involved, so that it can take necessary measures to prevent or delay as much degradation.[2] Silicones can be degraded, mainly at elevated temperatures, in presence of compounds able to act as depolymerisation catalysts.[3] However, the hydrophobic nature of silicones limits their contact with many aqueous solutions and allows their use in the presence of many chemical compounds. These factors, besides UV transparency confer them outstanding weathering resistance.[4] It has been shown that the main chemical reaction that occurs during

ageing of silicone rubber is oxidation with formation of by-products of oxidation.[5] Thermal stability of the silicones in general and polydimethylsiloxane (PDMS) in special, either in raw or crosslinked state or containing different additives was studied by a number of research teams both in oxidative and inert atmosphere.[2,6–10] Photo-ageing studies on polysiloxanes were also carried out, [2,11–14] either by techniques such as densimetry and hardness measurements[15] or in differential scanning calorimetry (DSC) furnace and the results were discussed in comparison with those obtained by complementary techniques such as thermogravimetrical analysis (TGA) and gel permeation chromatography (GPC)[2]. It has been concluded that both thermal and photo-stability is influenced by the nature of organic substituent at the silicone atom (methyl, vinyl, phenyl, H, etc.). Exposure of silicone rubber to radiation has very similar effects to those caused by heat ageing leading to an increase in hardness and a decrease in both tensile and elongation.[16,17]

Marine medium is considered aggressive from chemical (high content of salts), physical (water pressure, wave power, temperature changes) and biological (attachment of bacteria and microalgae) points of view. Although aging in marine environment has been extensively investigated for some organic materials,[18–20] there are few reports about the behavior and aging mechanism of the elastomers such as silicone, in such an environment.[21–24] The processes that can occur in the marine environment are water absorption, hydrolysis, additive extraction, oxidation, in dependence on material nature and composition.[24–26] However, there are very few long term data available, which limits clear explanations of the ageing mechanisms involved.[24] Three different silicones formulated to have high refractive index were subjected to accelerated ageing tests differing by light source, humidity, temperature, time. The results indicated in general a good survival of the original properties but in dependence on silicone compositions.[27] Other ageing tests on the silicone rubber outdoor polymer insulator under salt water based on a standardized procedure (dip wheel, continuous 30 000 test cycles) revealed decreasing in hydrophobicity and increasing in hardness.[28]

In this paper we studied the ageing of a series of silicone-barium titanate composites. We have developed these composites in a larger study aiming the optimization of the silicones mainly in terms of mechanical and dielectric properties for use as dielectrics in wave energy harvesting units. We chose barium titanate as filler for silicones, which is one of the most researched dielectric materials, due to its high dielectric permittivity and low loss characteristics. In addition, it can be easily prepared and used, being chemically and mechanically very stable.[29,30] Barium titanate powder of high purity is reported to be a key component in applications, such as energy storage capacitors and multilayer capacitors.[29,31]

Considering the fact that these materials will be an essential part of ocean energy recovery devices that should work as long as possible in a marine environment, we considered appropriate to assess their behavior in such an environment. For this purpose, the composites were immersed for one year in artificial sea water mainly in static conditions with intermittent back and forth movements (protocol B). Similar samples extracted after half year from saline water were further exposed to UV radiation (protocol A). The changes occurred in the morphology, thermal, mechanical and dielectric properties

were monitored from time to time. Similar studies have been reported in literature but on other types of composite (i.e., epoxy resins reinforced with glass fiber,[32,33] carbon fiber / epoxy composites.[34,35] We started from the premise that hydrophobic silicone matrix will limit water sorption, which is the key issue in ensuring the long term stability of polymer matrix composites.[34,36,37]

2. Experimental

2.1. Materials

The polydimethylsiloxane-α,ω-diols, PDMSs, of molecular masses as presented in Table 1 were synthesized according to the already described procedures:[38,39] cationic ring-opening polymerization of octamethylcyclotetrasiloxane in the presence of a cation exchanger as catalyst (PDMS with Mn=40 000 g/mol), and H_2SO_4 (for PDMS with Mn 235 000 and 650 000 g/mol). Barium titanate, ($BaTiO_3$), BT, with particle size <3 μm and PLURONIC L-31, HO-poly(ethyleneglycol)-*block*-poly(propyleneglycol)-*block*-poly(ethyleneglycol)-OH (M=1100 g/mol, d_{25}^{25} = 1.02) were purchased from Fluka AG. Methyltriacetoxysilane (MTAS) has been prepared by a procedure adapted from the literature[40] as described in ref.[41] (b.p. =94-97 ^{o}C, d_4^{20} = 1.17, freezing point - 40 ^{o}C). The artificial sea water (ASW) used for ageing was prepared with distilled water and 3.3 wt% salt from SOLARIS PLANT S.A. without iodine addition.

2.2. Preparation procedure

The dielectric silicone composite films were prepared based on components whose amounts are presented in Table 1 and according to procedure described in ref.[42] Thus, pre-established amounts of barium titanate powder were mixed with surfactant PLURONIC L-31. Chloroform (10 ml) was added to obtain a less viscous mixture, which was both mechanically shaken (30 min) and by ultrasound (30 min) and afterwards this mixture was transferred over PDMS. Then, MTAS crosslinker was added and stirred thoroughly until the components formed a homogenous mixture. The resulted mixture was sonicated for 10 minutes in order to remove all the air bubbles trapped and was poured in a Teflon mold (15x5 cm) to obtain films of about 0.5-1 mm thickness. The samples were maintained in air, at room temperature, for 24 h and subsequently the formed films were easily detached from the substrate. The free standing films were then kept in the laboratory environment about one month for ageing before characterization by different techniques.

2.3. Accelerated ageing protocol

The samples, prepared according to the recipes presented in Table 1, were subjected to an accelerated ageing process by their immersion in artificial sea water (ASW) at room temperature and sunlight. Two series containing three pieces of film of each sample were immersed vertically being fixed with staples on pillars existing in artificial sea water bath as in Figure 1. The bath having immersed samples was subjected from time to time moving back and forth for several hours thus creating a wave-like motion of the water. One of the two series of samples was extracted from this after half a year and further subject to UV irradiation for 500 h (protocol A), while the other was maintained in ASW until one year (protocol B).

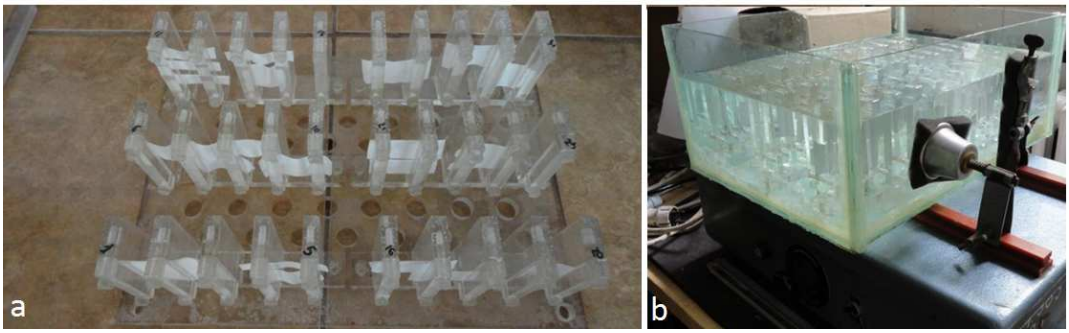

Fig. 1 Photo of the saline ageing bath.

Table 1 Recipes used for preparation of dielectric elastomeric composites

Sample	Mn, g/mol	PDMS, g	BT, g	Pl L31, mL	MTAS, g
M3BT10	650000	5	0.50	0.50	0.0015
M3BT15	650000	5	0.75	0.75	0.0015
M2BT10	235000	5	0.50	0.50	0.0040
M2BT15	235000	5	0.75	0.75	0.0040
M1BT10	40000	5	0.50	0.50	0.0230
M1BT15	40000	5	0.75	0.75	0.0230

2.4. Techniques

Filler treatment with surfactant and homogenization of the composites before curing were done in a highly intensive ultrasonic bath, Sonoreactor UTR200 (Hielscher Ultrasonics GmbH) with a maximum power density 80 W/cm^2, at an amplitude of 60 % and pulse mode ratio 0.5 cycles. UV radiation exposure was made in a laboratory chamber (Angellantoni Ind., Italy), with a mercury lamp (λ = 200 - 700 nm, incident light intensity of 39 mW cm^{-2}), at a temperature of 30 ^{o}C and humidity of 60%, for a period of 500 h. FTIR spectra were recorded with a Bruker Vertex 70 FTIR spectrometer in transmission mode on crushed sample by grinding and incorporated into KBr pellets. Raman spectra were recorded in the vibrational frequencies range 100-3250 cm^{-1} by using a Renishaw InVia Reflex spectrometer with a 632.8 nm HeNe laser as excitation source, 10 % power. The laser beam was focused on the film sample and the backscattered Raman signal with a 50x objective lens having a numerical aperture of 0.75 of a Leica DM 2500M microscope. The laser exposure was 10 s. The samples were investigated at low incident laser power in order to avoid sample degradation. Wide Angle X Ray Diffraction - WAXD was

performed on a Diffractometer D8 ADVANCE (Bruker AXS, Germany), using the Cu-Kα radiation (λ = 0.1541 nm), a parallel beam with Gobel mirror and a Dynamic Scintillation detector. The working conditions were 40 kV and 30 mA, 2s/step, 0.01 degree/step. All the diffractograms were investigated in the range 20-65.2 theta degrees, at room temperature. Scanning electron microscopy (SEM) images were acquired with an electronic microscope type Quanta 200 operating at 30 kV with secondary and backscattering electrons in low or high vacuum mode. Stress–strain measurements were performed on TIRA test 2161 apparatus, Maschinenbau GBTH Ravenstein, Germany on dumbbell-shaped cut samples with dimensions of 50x8.5x4 mm. Measurements were run at an extension rate of 20 mm/min, at room temperature. Cyclic tensile stress tests were performed on the similar samples between 2 and 100 % strain. Five stretch-recovery cycles were registered. The stationary time at minimum and maximum applied stress was 5 s. Dielectric spectroscopy was performed using the Novocontrol "Concept 40" broadband dielectric spectrometer (Hundsangen, Germany), at room temperature in the frequency domain 1 Hz–1 MHz. Differential scanning calorimetry (DSC) measurements were conducted on a DSC 200 F3 Maia device (Netzsch, Germany). A mass of 10 mg of each sample was heated in pierced and sealed aluminum crucibles in nitrogen atmosphere at a flow rate of 50 mL·min^{-1} and a heating rate of 10 ^{o}C·min^{-1}. The temperature against heat flow was recorded. The baseline was obtained by scanning the temperature domain of the experiments with an empty crucible. The instrument was calibrated with indium at various heating rates according to standard procedures.[43]

3. Results and discussions

Six formulations of PDMS-BT composites differing by molecular weight of the PDMS (Mn 40000, 235000 and 650000) as well as BT content (10 and 15 pph) were prepared (Table 1). After dispersion with surfactant in chloroform medium, BT was incorporated within silicone matrix by mechanical mixing. The homogenized mixtures were processed as films that were stabilized by crosslinking with methyltriacetoxysilane at room temperature according to well-established procedure.[42] The films aged in laboratory conditions were immersed in ASW, part of them for one year (protocol B) and another part for half year. For the second part, the ageing procedure was continued in dry state under the influence of UV-Vis radiation (protocol A). Both initial and aged films were analysed by different techniques (FTIR and Raman spectroscopy, WAXD, SEM, mechanical testing, dielectrical spectroscopy, DSC) in order to evaluate the modifications produced in their structure and properties as a result of the exposure in the above presented conditions.

All samples, regardless of the state they are in (non-aging, subjected to protocol A or B) show very similar FTIR spectra without indicating structural changes. Thus, in all spectra are present bands from about 1020 to 1100 cm^{-1} (Si-O-Si stretch), 800 cm^{-1} (CH_3 asymmetric rocking, Si-C asymmetric stretch), 1260 cm^{-1} (CH_3 symmetric bending), 2966 cm^{-1} (CH_3 asymmetric stretch) and 2920 cm^{-1} (CH_3 symmetric stretch).[44] The strong bands around 3400 and 1620 cm^{-1} in some spectra are due to present atmospheric water due to insufficient compaction of the sample in KBr pill. FTIR spectra recorded for three of the composites in the

three stages (initial, aged according to Protocol A and B) are demonstrative shown in supporting information as Figures 1S-3S (Supporting information).

In Raman spectra of the samples in the three stages (Figure 4S) there are visible intense bands at 2966 and 2906 (CH_3 asymmetric and symmetric stretch, respectively), 708 and 490 (Si-O-Si stretch) and very weak bands at 1260 and 1406 cm^{-1} (CH_3 symmetric and asymmetric bending, respectively)[44] without significant differences between them. The bands at 187, 226, and 306 cm^{-1} are due to barium titanate.[45] The Raman bands corresponding to the surfactant used, which should occur at around 2975, 2930 and 2875 cm^{-1} overlaps with the peaks corresponding to PDMS, and due to their low intensity, those that should be at 1455, 1350 and 875 cm^{-1} are also not seen in spectra.

X-ray diffraction patterns recorded at room temperature on films for initial samples and those aged under protocol A and protocol B, respectively, are also identical (Figures 2, 5S and 6S). The diffraction peaks correspond to the barium titanate[45] (Table 1S), silicone matrix being, as is well known, amorphous at room temperature.

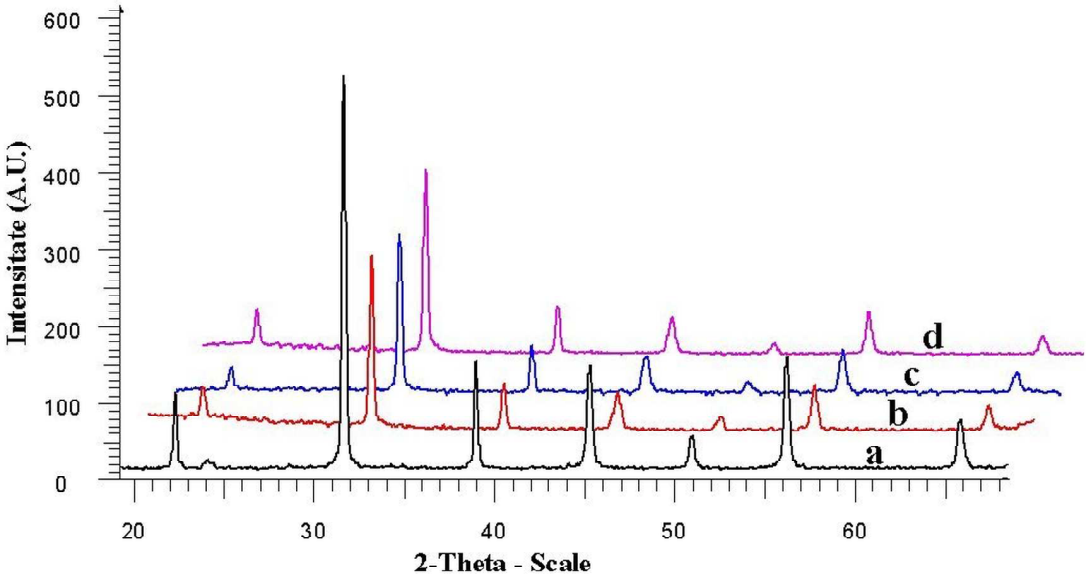

Fig. 2 WAXD patterns for: a-barium titanate as compared with sample M2BT10: b - no-aging; c - aged according to protocol A; d - aged according to protocol B.

On the *SEM images* taken on the initial film surfaces, it may be noticed the existence of spherical formations consisting of BT aggregates encapsulated in surfactant, dimensional polydisperse from very small to several microns (Figure 3a). Islands of surfactant without BT are also visible. After immersion in ASW, half a year and UV irradiation 500 h, changes occur on the surface of the films. Barium titanate aggregates become more visible besides deposited sodium chloride crystals, while surfactant domains are still present (Figure 3b). Instead, after one year of stay in ASW, some surface erosion is observed due

to the surfactant extraction (Figure 3c). It is presumed that in the high polar medium or/and UV light exposure, the film surface reorganizes leading to considerable increases in its hydrophilicity and rugosity as has also been revealed by other studies.[46] EDX analysis reveals the presence of Na and Cl besides the other expected elements, O, Si, Ba and Ti, on the surface of the film (Figure 7S). After extraction with distilled water, one can see the imprint left on the surface film by sodium chloride crystals as track of their dissolution (Figure 3d). EDX analysis confirms the absence of Na and Cl on the film surface after washing (Figure 8S). By analyzing again the EDX data of the samples as were removed from ASW (Figure 7S), it can be seen that in samples containing a larger amount of surfactant, such as those of MBT15 (amount of surfactant incorporated is equal to that of BT as shown in Table 1), a greater amount of chloride and sodium was found both on surface and in section. In the case of sample M2BT10 where a lower amount of surfactant was used, the natrium chloride deposited on the outer surface or migrated into the sample is in very little amount (much below one percent). On this basis, we can opine that the surfactant is one that favors both sodium chloride deposition on the surface and its migration inside the film. Also the amount of natrium chloride elements identified by EDAX within the samples increase when the immersion time in ASW is greater. A modification of the *mechanical properties* of the polymers is to be expected as a result of their marine ageing due to water infiltration and degradation of the filler-matrix interface.[47] In the case of silicones, these effects should be less visible due to their known high hydrophobicity. Stress-strain curves of the original samples (Figure 4a) reveal that the molecular masses along with filler percentage have a great influence on the mechanical behaviour of the composites. Thus, the mechanical strength increases from 0.23 MPa in the M3BT series to 0.41 MPa in the M1BT one, while the maximum strain decreases from 1150 to 151%, respectively (Table 2). The difference is greater between the M2BT and M1BT series where molecular mass decreases almost six times, from 235 000 to 40 000. This behavior is expected because the crosslinking density increases as the molecular weight decreases due to the crosslinking performed through chain ends with a trifunctional silane, and the possibility of the chains to slide past each other is reduced. Sample M3BT10, having 10% BT, has a maximum strain of 1150 %. Increasing the amount of BT at 15 wt%, this drastically decreases to 374 %. In the M2BT series, this decrease is rather moderate one, from 594 % to 455 %, while in the M1BT one there is even a slight increase from 113 to 151 %.

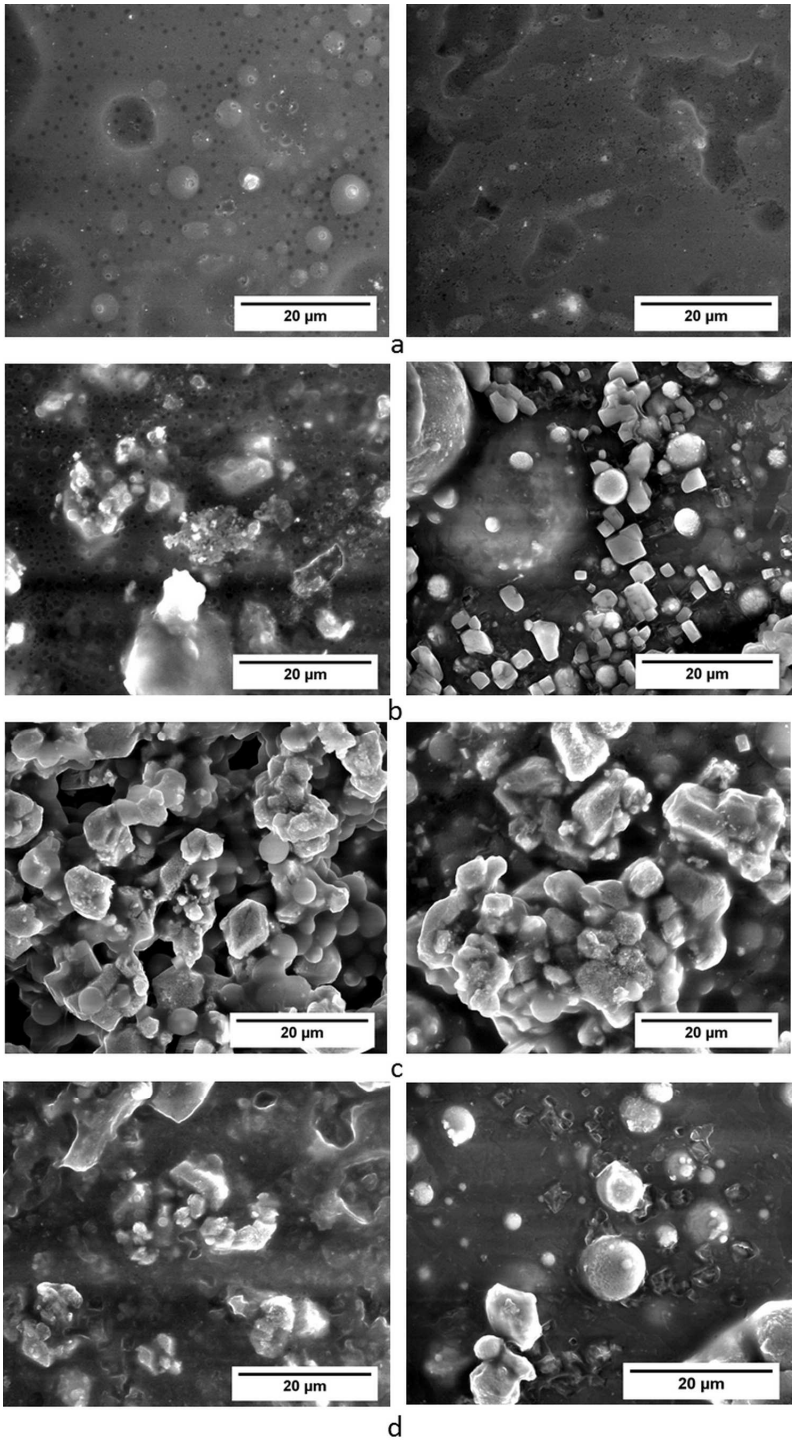

Fig. 3 SEM images of M2BT15 (left) and M1BT10 (right) samples in different stages: a – original; b - aged half year in ASW and 500 h UV irradiated; c – aged one year in seawater; d – extracted in clean water.

The test results for mechanical fatigue resistance, at strains up to 100 % of initial length, show an elastic behaviour in all cases with a clearly visible hysteresis loop only at the first strain-release cycle when the siloxane chains are rearranged in the film and the difference between strain and release was smaller than 1% of the stress value at each point (Figure 4b). In fact, this behaviour might be associated with Mullins effect (first-cycles stress-softening),[48] which are more visible for the series M3BT based on the highest molecular mass elastomers.

Table 2 Relevant mechanical and dielectric characteristics for tested samples

Ageing Type	Characteristic	Sample					
		M3BT10	**M3BT15**	**M2BT10**	**M2BT15**	**M1BT10**	**M1BT15**
No ageing	σ, MPa	0.23	0.2	0.29	0.24	0.39	0.41
	ε, %	1150	374	594	455	113	151
	E, MPa	0.10	0.05	0.25	0.08	0.66	0.36
	ε'	4.95	5.89	4.41	5.07	3.78	5.03
	ε''	0.036	0.017	0.068	0.075	0.160	0.038
	UTT,[a] KJ/m^3	17.46	5.35	9.88	6.79	2.78	3.90
Protocol A ageing	σ, MPa	0.18	0.19	0.23	0.36	0.69	0.52
	ε, %	240	252	234	272	78	123
	E, MPa	0.23	0.22	0.25	0.31	0.9	0.58
	ε'	3.57	4.23	3.72	3.9	3.57	3.76
	ε''	0.017	0.016	0.1	0.016	0.042	0.13
	UTT,[a] KJ/m^3	3.06	3.26	3.51	6.11	2.98	3.59
Protocol B ageing	σ, MPa	0.29	0.31	0.55	0.6	0.45	0.45
	ε, %	806	763	435	422	76	100
	E, MPa	0.025	0.16	0.40	0.40	0.60	0.72
	ε'	10.55	5.61	13.07	4.87	3.26	4.37
	ε''	51.92	18.063	147.23	4.41	0.26	0.12
	UTT,[a] KJ/m^3	15.53	15.21	13.89	15.01	1.70	2.82

[a] Ultimate tensile toughness

A drastic decrease of the elongation is observed when the samples were submitted to protocol A ageing (Figure 4c, Table 2). It is well-known that silicones present UV resistance, but the surfactant used is not stable under UV irradiation. Pluronic L31 is an amphiphile copolymer that acts like a surfactant with the hydrophilic part, poly(ethyleneglycol), oriented to the polar hydrophilic barium titanate particles while the hydrophobic blocks are oriented in the opposite direction to hydrophobic silicone matrix, thus assuring the compatibilization of the two components and good dispersability of the particles within continue silicone phase. Thus, due to surfactant degradation, the filler is no longer compatible with the matrix and the maximum elongation decrease. The elastic properties are not changed during this ageing (Figure 4d). After one year in saline water only, almost all samples show around 30% decreasing in the maximum elongation values (Figure 4e, Table 2), while the mechanical strength significantly increases, the more the higher the molecular weight of the polymer matrix. This could be due to partial extraction of the surfactant. M3BT and M2BT series still maintain high elongation that suits from this point of view for energy harvesting (more than 400%, up to 800%). The elastic properties are not affected, moreover for M3BT series the hysteresis loop disappears (Figure 4f). The domains characteristic for perfectly elastic materials within the samples behaviour were estimated on the basis of linear part of the stress-strain curves and are provided in Table 3 as strain and elasticity modulus values. As expected, elastic modulus increases by decreasing the molecular mass of the polymeric matrix, while the elongation limits slightly decrease. An increasing in elasticity modulus is also registered as a result of the ageing processes either by protocol A or protocol B, the elongation remaining almost in the same range values.

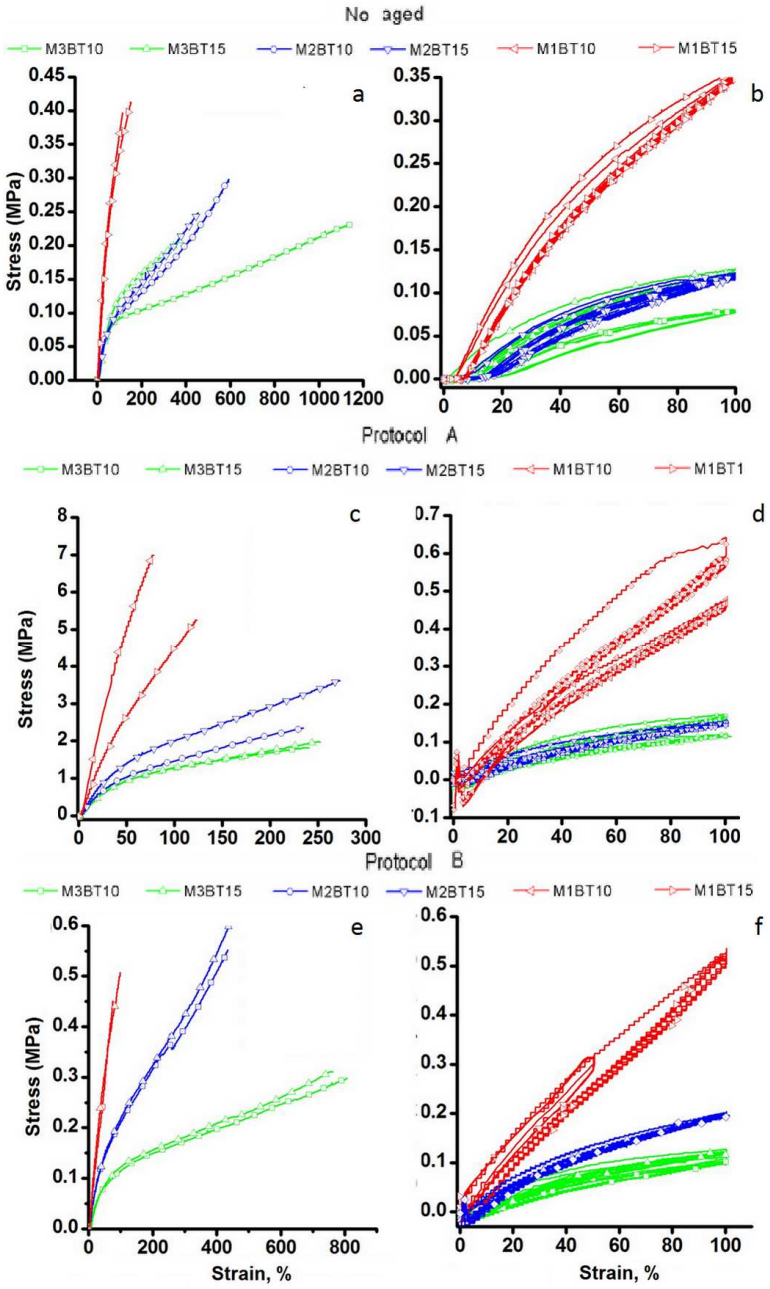

Fig. 4 Normal (left) and cyclic (right) stress-strain curves for non-aged (a, b), aged according to protocol A (b, c) and aged according to protocol B (d, e) samples.

Table 3 Permanent set values for initial samples and after ageing

	Original samples		Protocol A ageing		Protocol B ageing	
	Strain, %	E, MPa	Strain, %	E, MPa	Strain, %	E, MPa
M3BT10	24.0	0.178	23.1	0.244	19.4	0.232
M3BT15	25.0	0.248	22.4	0.242	19.0	0.200
M2BT10	15.0	0.247	22.8	0.266	22.5	0.357
MTBT15	23.5	0.165	23.4	0.358	22.7	0.378
M1BT10	12.3	0.658	23.6	1.070	26.5	0.566
M1BT15	19.7	0.491	25.1	0.626	26.0	0.673

While the strength indicates how much force the material can support, the tensile toughness is a measure of the amount of energy per volume that a material can absorb to failure and is estimated as area under tensile stress-strain curves (Table 2).[49–51] The values of the area integrated under the entire stress-strain curve, to the break point, known as ultimate tensile toughness (UTT), are graphically presented for both our original and aged samples in Figure 5. As it is known, in order to be tough, a material must be both strong and extensible. If we analyze the entire spectrum of stress-strain curves, and taking into account the structure and composition of the materials, it would be expected as the balance to be best met by the samples based on PDMS having molecular mass of 235000 g/mol (M2BT series). The samples based on the highest molecular mass PDMS (650000 g/mol) (M3BT series) possess low crosslinking density that results in high elongation and low brittleness while the samples from M1BT series, which are based on the lowest molecular mass PDMS (40000 g/mol), are strong but have weak stretching capability. Excepting the original M3BT10 sample, which shows the highest UTT value, 17.46 kJ/m^3, this expectation is confirmed. The values for the original M2BT series are larger (9.88 and 6.79 kJ/m^3) as compared with the other samples, M3BT15 (5.35 kJ/m^3) and M2BT1 series (2.78 and 3.90 kJ/m^3). However, these values are lower as compared with those reported in literature for examples, for stronger polystyrene and ethylene-styrene interpolymers, and estimated on the same bases, when they are ranging between 9 and 61 MJ/m^3 in dependence on composition.[51] On silicones, we found in literature the fracture energy estimated for commercial ZruElast™ A1040 to be 6.15 kJ/m^2.[52] This suggests that our material would be suitable for harvesting rather low energies. Instead they have the advantage of a good weathering behaviour if properly formulated (eg, avoid using surfactants). By ageing according to

protocol A, significant decrease of the thoughness occurs for the samples M2BT and M3BT (3.06 – 6.11 kJ/m^3), while by applying protocol B, the values for these samples are significantly higher (13.89-15.53 kJ/m^3). The M1BT series having the lowest toughness values seems to be the least affected by the ageing process.

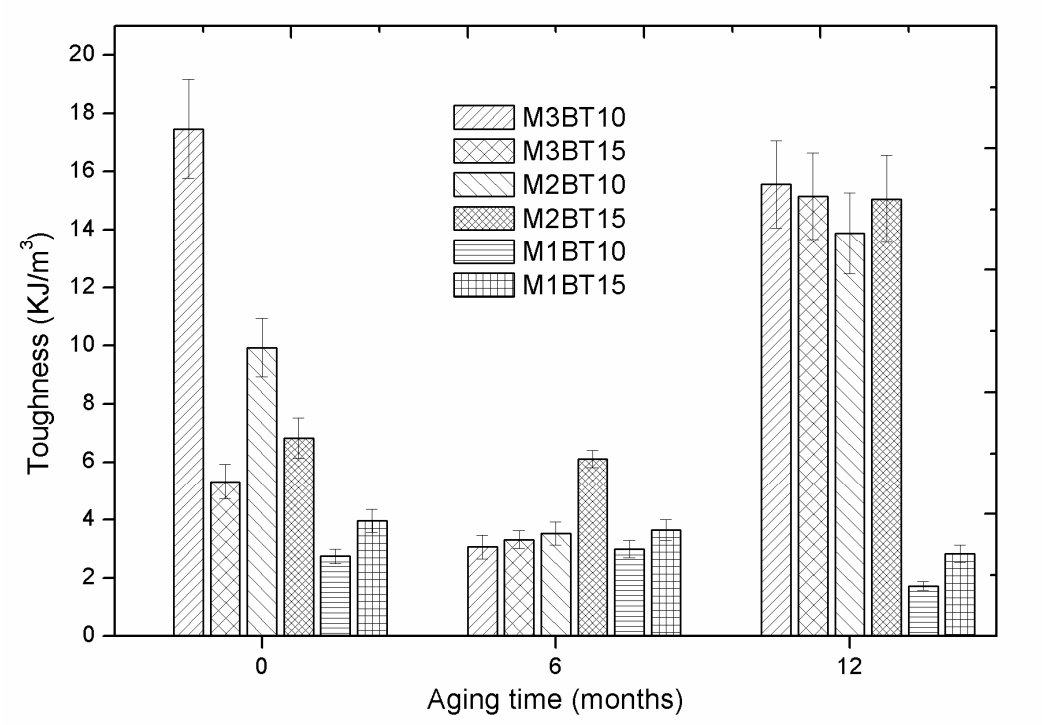

Fig. 5 The ultimate tensile toughness values in dependence on the ageing state for the prepared samples.

Other values of absorbed energy from an integration of partial stress-strain curves have no standard name. Although it is not a common practice, we evaluated the toughness at 100 % elongation on cyclic stress-strain curves of the original samples as an indirect measure of the energy that the elastic material could release when force that acted on it was removed like in a harvesting energy system. If we analyse the values presented in Table 4, we can see that the M1BT samples show significantly higher toughness values as compared with M2BTs and M3BTs. Concerning to the effect of the barium titanate content, its enhancing effect for 5 wt% leads to an increase in toughness with about 3 % in M1BTs but with about 72 % in M3BTs, probably as a result of BT contribution mainly to reduce the extensibility of the sample. Excepting the first cycle, the toughness estimated on the basis of the other cycles is almost unmodified in all cases.

Table 4. Absorbed energy (KJ/m^3) by the original samples at 100% elongation for 5 stress-strain cycles

Cycles	M3BT10	M3BT15	M2BT10	M2BT15	M1BT10	M1BT15
1	0.45	0.85	0.71	0.74	2.06	2.18
2	0.43	0.73	0.67	0.66	1.89	1.95
3	0.43	0.71	0.66	0.64	1.88	1.92
4	0.42	0.70	0.65	0.64	1.88	1.91
5	0.42	0.70	0.65	0.63	1.87	1.90

As expected, the *dielectric permittivity* for samples without ageing increases by incorporation of barium titanate, a dielectric ceramic. Thus, while pure crosslinked PDMS have ε'~3 at 10 Hz, increases up to 4.95 and 5.89 for M3 series, 4.41 and 5.07 for M2 series, 3.78 and 5.03 for M1 series was observed. Comparing the samples containing the same amount of BT, we can conclude that even the polymeric matrix has a contribution, from 3.78 up to 4.95 for samples with 10% BT (Figure 6a, Table 2). There is a sudden drop at about 10^3 Hz for ε`, accompanied with the maximum dielectric loss, ε" (Figure 6b), suggesting a relaxation process occurring at silicone-filler interface. The decrease in the dielectric permittivity is due to the inability of the dipoles to return to its original random orientation, known as relaxation time, which is larger than the rate of oscillating electric field.

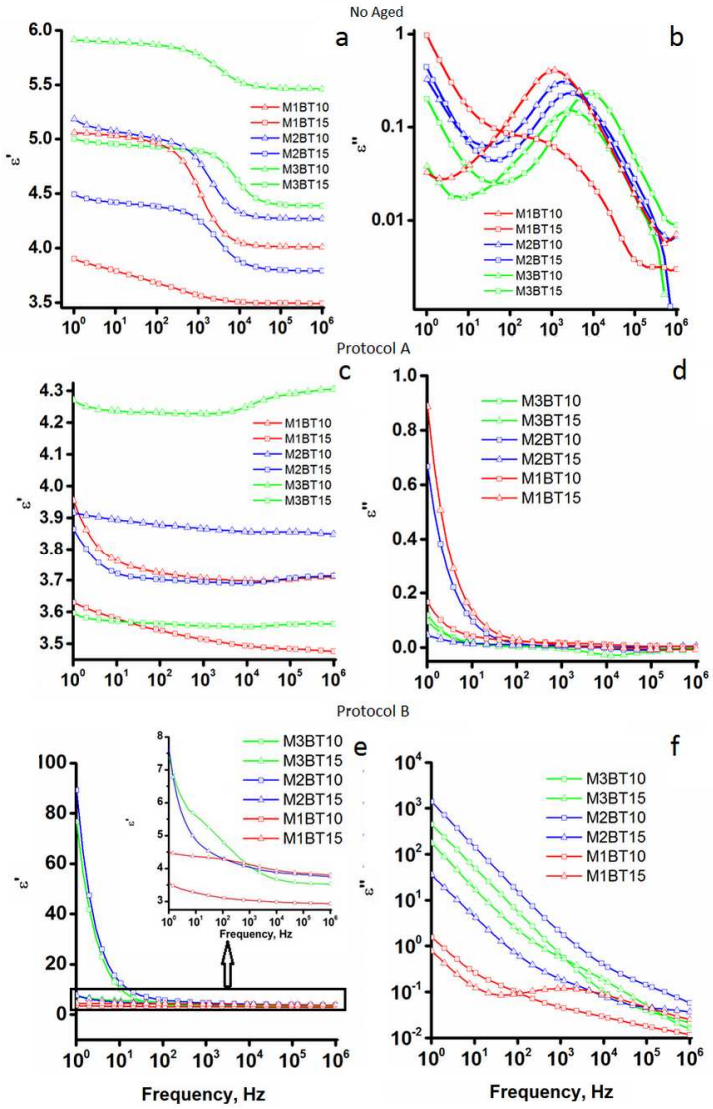

Fig. 6 Frequency variation of dielectric permittivity (left) and dielectric losses (left) for samples without ageing (a, b), after being subjected to aging according to protocol A (c, d) and protocol B (e, f).

After protocol A ageing (Figure 6c, d, Table 2), slight decreases in dielectric permittivity and dielectric loss are observed and, moreover, stabilization at high frequencies occurs. After one year in saline water (protocol B) along with an increase in permittivity, a high increase in dielectric loss was observed for M3BT and M2BT series (Figure 6e, f, Table 2), due to the salt ions that migrate inside films (Figure 7S). For M1BT series a small decrease both in dielectric permittivity and dielectric loss can be noticed. However, the conductivity-frequency curves (Figure 9S) show that all samples are maintained in semiconductor (10^{-18} - 10^{-8} S/cm) field regardless of the ageing process in which they were submitted.

Differential scaning calorimetry analysis results (Figure 10S) reveal the glass transition values for the initial samples in the range -123- (-120) ^{o}C. Unsignificant variations occur as a result of ageing. However, larger changes are registered for the crystallization degree, χ_c (Figure 7), evaluated on the basis of DSC curves (calculated with the equation $\Delta Ht_2/ \Delta H_{literature}$, where $\Delta H_{literature}$ = 61.3 J g^{-1} [53–55] in dependence on the polymeric matrix structure). As can be observed in Figure 7, it decreases with decreasing molecular weight of the polymer matrix. This is normal behavior because here the crosslinking degree is higher, thus limiting the degree of freedom of the chain to adopt ordered conformations. No significant changes develop in the degree of crystallinity of the samples due to variation in the filler content or due to their submission to the two accelerated ageing processes.

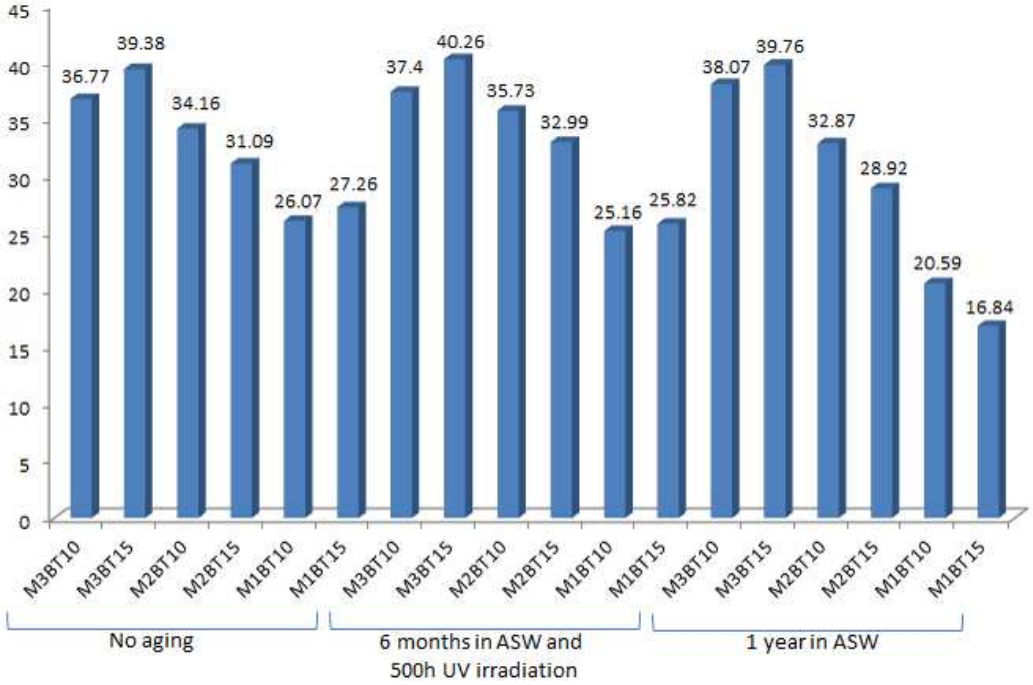

Fig. 7 Crystallization degree, χ_c, for M1BT, M2BT, and M3BT series.

4. Conclusions

Six silicone composite samples differing by the molecular masses of the matrix polymers as well as by the content of barium titanate incorporated were crosslinked by condensation with methyltriacetoxysilane in form of films. These were aged either by immersion in artificial seawater for one half year followed by UV irradiation for 500 h (protocol A) or one year only in saline water without irradiation (protocol B). A slight erosion of the surface occurred as a result of these treatment regimes due both to the physical organization of the hydrophobic siloxane chains and to the extraction of the surfactant. The mechanical characteristics are significantly affected when protocol A was applied, while the dielectric permittivity is mainly affected by a longer exposure to seawater only (protocol B). Although the analyses by FTIR and Raman spectroscopies

as well as by WAXD not evidenced structural changes of the composites as a result of their exposure in established conditions, it seems that the presence of surfactant used for dispersing the filler in the polymer matrix has negative effects on the ageing process favoring the deposition of salt on the surface of the film and even migration inside it. The degree of crystallinity is influenced by the chain length and not the filler content nor the ageing process on which the sample was subjected. The tensile toughness values determined from cyclic stress-strain curves elongated up to 100% suggests a greater capacity to harvest energy for the samples based on the lower molecular weight polymer.

Acknowledgements: The work presented in this paper is developed in the context of the project PolyWEC (www.polywec.org, prj. ref. 309139), a FET-Energy project that is partially funded by the 7th Framework Programme of European Community and co-financed by Romanian National Authority for Scientific Research, CNCS-UEFISCDI (Contract 205EU). Thanks dr. Iuliana Spiridon who allowed us access to UV irradiation aging chamber, and dr. Elena-Laura Ursu for recording Raman spectra.

Notes and references

1 N. Gharavi, M. Razzaghi-Kashani and N. Golshan-Ebrahimi, *Smart Mater. Struct.*, 2010, **19**, 025002.

2 N. S. Tomer, *Open J. Org. Polym. Mater.*, 2012, **02**, 13–22.

3 T. Tadros, *Encyclopedia of Colloid and Interface Science*, Springer, Wokingham, Berkshire, 2013.

4 A. Colas, *Silicones: Preparation, Properties and Performances,*Dow Corning Life Sci., 2005, 1-14.

5 B. H. Chudnovsky, *Electrical Power Transmission and Distribution: Aging and Life Extension Techniques*, CRC Press, 2012.

6 N. Grassie, K.F. Francey and I. G. Macfarlane, *Polym. Degrad. Stab.*, 1980, **2**, 67–83.

7 C. Camino, S. M. Lomakin and M. Lazzari, *Polymer*, 2001, **42**, 2395–2402.

8 G. Camino, S. M. Lomakin and M. Lageard, *Polymer*, 2002, **43**, 2011–2015.

9 E. Vallés, C. Sarmoria, M. Villar, M. Lazzari and O. Chiantore, *Polym. Degrad. Stab.*, 2000, **69**, 67–71.

10 T. H. Thomas and T. C. Kendrick, *J. Polym. Sci. Part -2 Polym. Phys.*, 1969, **7**, 537–549.

11 Y. Israeli, J. Lacoste, J. Cavezzan and J. Lemaire, *Polym. Degrad. Stab.*, 1995, **47**, 357–362.

12 Y. Israeli, J.-L. Philippart, J. Cavezzan, J. Lacoste and J. Lemaire, *Polym. Degrad. Stab.*, 1992, **36**, 179–185.

13 Y. Israëli, J. Cavezzan and J. Lacoste, *Polym. Degrad. Stab.*, 1992, **37**, 201–208.

14 Y. Israëli, J. Lacoste, J. Cavezzan and J. Lemaire, *Polym. Degrad. Stab.*, 1993, **42**, 267–279.

15 F. Virlogeux, D. Bianchini, F. Delor-Jestin, M. Baba and J. Lacoste, *Polym. Int.*, 2004, **53**, 163–168.

16 K.-C. Cheng, C.-M. Lin, S.-F. Wang, S.-T. Lin and C.-F. Yang, *Mater. Lett.*, 2007, **61**, 757–760.

17 P. J. Flory and J. Rehner, *J. Chem. Phys.*, 1943, **11**, 521.

18 N. Guermazi, K. Elleuch and H. F. Ayedi, *Mater. Des.*, 2009, **30**, 2006–2010.

19 E. Legghe, E. Aragon, L. Bélec, A. Margaillan and D. Melot, *Prog. Org. Coat.*, 2009, **66**, 276–280.

20 J. Unsworth and Y. S. Ng, *Internationnal conference on Polymers in a marine environments,* 1984, **97**, 73-76.

21 K. Ab-Malek and A. Stevenson, *J. Mater. Sci.*, 1986, **21**, 147–154.

22 D. Oldfield and T. Symes, *Polym. Test.*, 1996, **15**, 115–128.

23 M. Rutkowska, K. Krasowska, A. Heimowska, I. Steinka and H. Janik, *Polym. Degrad. Stab.*, 2002, **76**, 233–239.

24 P. Y. Le Gac, V. Le Saux, M. Paris and Y. Marco, *Polym. Degrad. Stab.*, 2012, **97**, 288–296.

25 I. Merdas, F. Thominette and J. Verdu, *Polym. Degrad. Stab.*, 2003, **79**, 419–425.

26 P. H. Mott and C. M. Roland, *Rubber Chem. Technol.*, 2001, **74**, 79–88.

27 K. R. McIntosh, N. E. Powell, A. W. Norris, J. N. Cotsell and B. M. Ketola, *Prog. Photovolt. Res. Appl.*, 2011, **19**, 294–300.

28 Y. X. Zhou, Q. Nie, Z. Z. Chen and R. Liu, *J. Phys. Conf. Ser.*, 2009, **183**, 012013.

29 M. M. Vijatović, J. D. Bobić and B. D. Stajanovic, *Sci. Sinter.*, 2008, **40**, 155–165.

30 F. Jona G. Shirane, *Ferroelectric Crystals*, Dover Publications, New York, 1993.

31 P. Kim, S. C. Jones, P. J. Hotchkiss, J. N. Haddock, B. Kippelen, S. R. Marder and J. W. Perry, *Adv. Mater.*, 2007, **19**, 1001–1005.

32 D. Miller, J. F. Mandell, D. D. Samborsky and B. A. Hernandez-Sanchez, *Performance of Composite Materials Subjected to Salt Water Environments*, Honolulu, Hawaii, 2012, 23–26.

33 A. Boisseau, P. Davies and F. Thiebaud, *Appl. Compos. Mater.*, 2011, **19**, 459–473.

34 G. Sala, *Compos. Part B Eng.*, 2000, **31**, 357–373.

35 I. F. Soykok, O. Sayman and A. Pasinli, *Compos. Part B Eng.*, 2013, **54**, 59–70.

36 P. Musto, M. Galizia, G. Scherillo and G. Mensitieri, *Durability of Composites in a Marine environment,* 2014, **208**, 15-45.

37 S. Samaržija-Jovanović, V. Jovanović, G. Marković, S. Konstantinović and M. Marinović-Cincović, *Compos. Part B Eng.*, 2011, **42**, 1244–1250.

38 M. Cazacu and M. Marcu, *J. Macromol. Sci. Part A*, 1995, **32**, 1019–1029.

39 M. Cazacu, C. Racles, A. Vlad, M. Antohe and N. Forna, *J. Compos. Mater.*, 2009, **43**, 2045–2055.

40 W. Noll, *Chemistry and technology of silicones*, Academic Press, New York and London, 1968.

41 A. Bele, M. Cazacu, G. Stiubianu and S. Vlad, *RSC Adv.*, 2014, **4**, 58522–58529.

42 A. Bele, M. Cazacu, G. Stiubianu, S. Vlad and M. Ignat, *Compos. Part B Eng.*, 2015, **68**, 237–245.

43 G. W. H. Höhne, H. K. Cammenga, W. Eysel, E. Gmelin and W. Hemminger, *Thermochim. Acta*, 1990, **160**, 1–12.

44 D. Cai, A. Neyer, R. Kuckuk and H. M. Heise, *J. Mol. Struct.*, 2010, **976**, 274–281.

45 Z. Lazarevic, N. Romcevic, M. Vijatovic, N. Paunovic, M. Romcevic, B. Stojanovic and Z. D. Mitrovici, Acta Phys. Pol., A, 2009, **115**, 808–810.

46 A. Favre, E. R. Fotsing and M. Levesque and E. Ruiz, *J Elastom Plast*, 2015, 1-9.

47 F. F. Estarlich, S. a Lewey, T. G. Nevell, A. a Thorpe, J. Tsibouklis and A. C. Upton, *Biofouling*, 2000, **16**, 263–275.

48 H. Zhao, D.-R. Wang, J.-W. Zha, J. Zhao and Z.-M. Dang, *J. Mater. Chem. A*, 2013, **1**, 3140.

49 M. A. Cole and C. N. Bowman, *J. Polym. Sci. Part Polym. Chem.*, 2012, **50**, 4325–4333.

50 C. P. Park, *J. Polym. Eng.*, 2001, **21**, 511-520.

51 D. Askeland, P. Fulay and W. Wright, *The Science and Engineering of Materials, SI Edition*, Cengage Learning, 2011.

52 R. Kaltseis, C. Keplinger, S. J. Adrian Koh, R. Baumgartner, Y. F. Goh, W. H. Ng, A. Kogler, A. Tröls, C. C. Foo, Z. Suo and S. Bauer, *RSC Adv.*, 2014, **4**, 27905.

53 C. M. Roland and Ca. Aronson, *Polym. Bull.*, 2000, **45**, 439–445.

54 J. Mark, *Polymer Data Handbook*, N. Y. USA, 1999.

55 L. Mandelkern and R. G. Alamo, *Physical Properties of Polymers Handbook*, J. E. Mark, Springer New York, 2007.

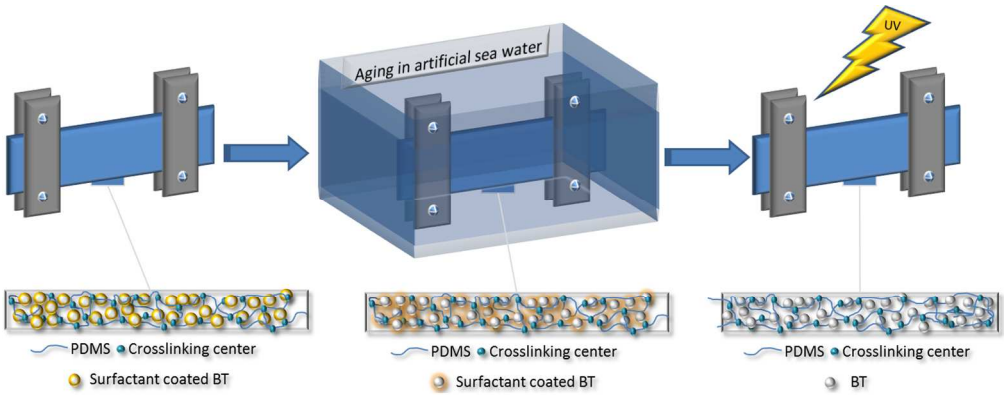

397x154mm (96 x 96 DPI)

Ageing behavior of the silicone dielectric elastomers in simulated marine environment

Adrian Bele, George Stiubianu, Stelian Vlad, Codrin Tugui, Cristian-Dragos Varganici, Lavinia Matricala, Daniel Timpu, Maria Cazacu

"Petru Poni" Institute of Macromolecular Chemistry, Aleea Gr. Ghica Voda 41A, 700487 Iasi, Romania

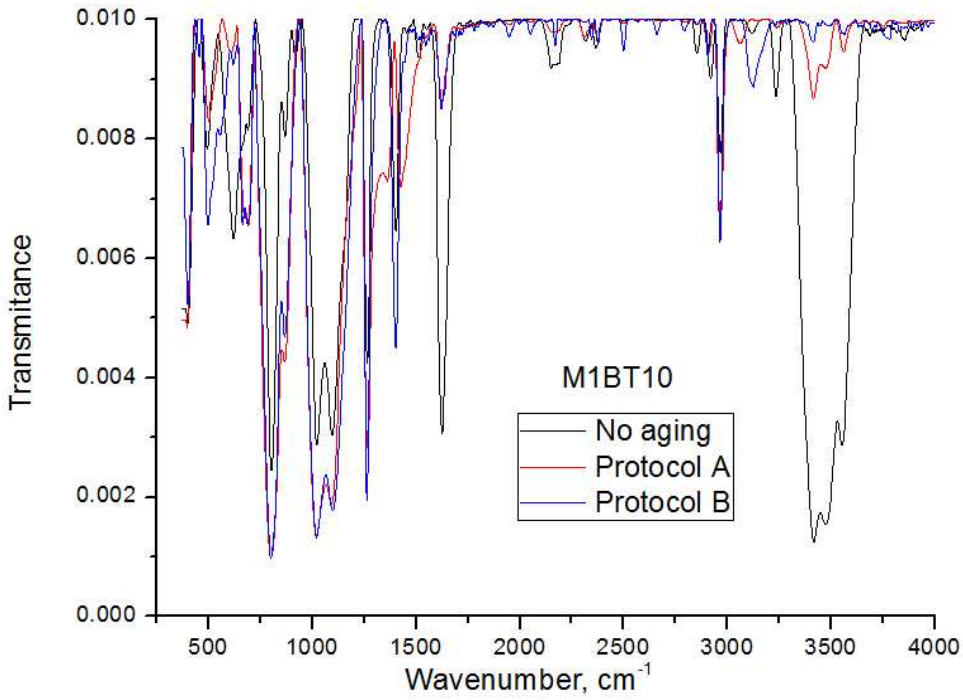

Figure 1S. Comparative FTIR spectra of the sample M1BT10, original and aging by protocols A and B.

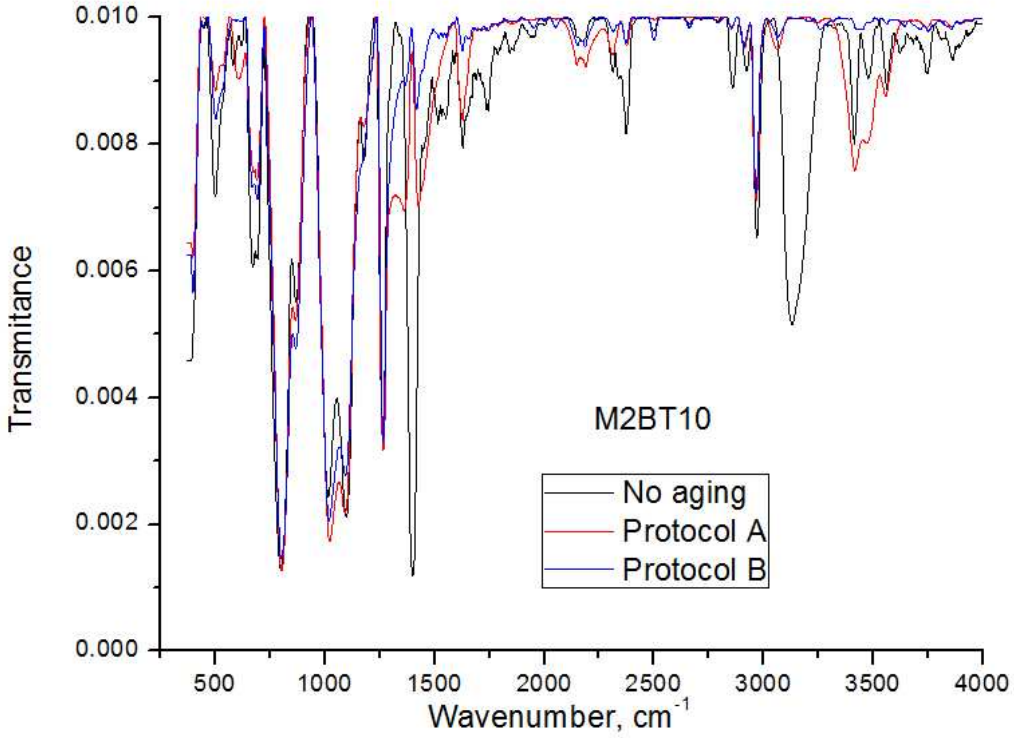

Figure 2S. Comparative FTIR spectra of the sample M2BT10, original and aging by protocols A and B.

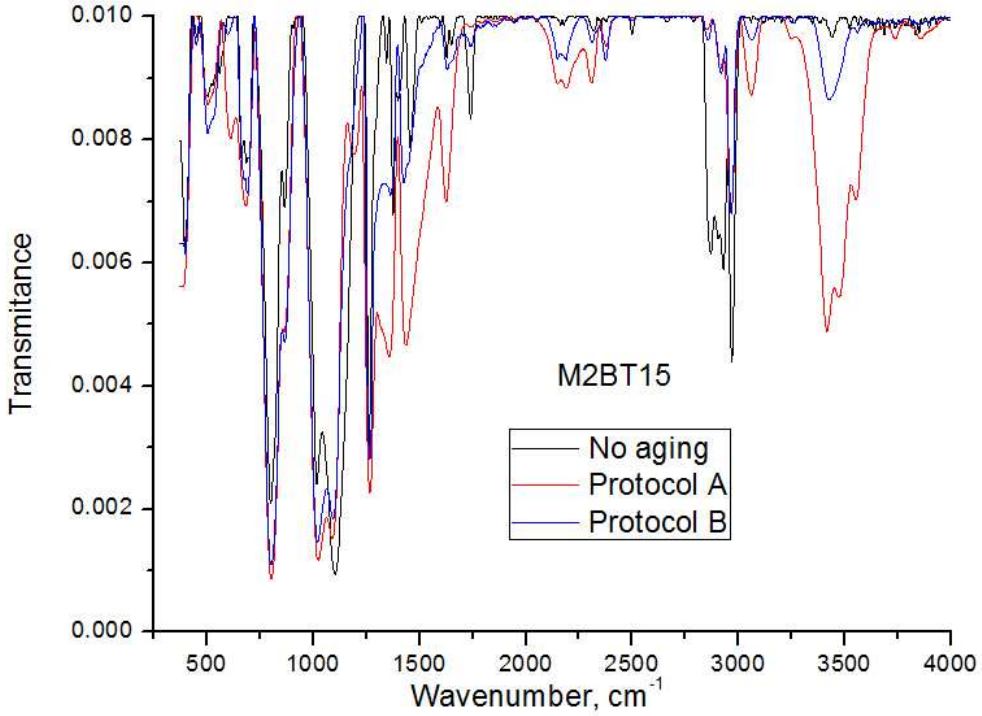

Figure 3S. Comparative FTIR spectra of the sample M2BT15, original adn aging by protocols A and B.

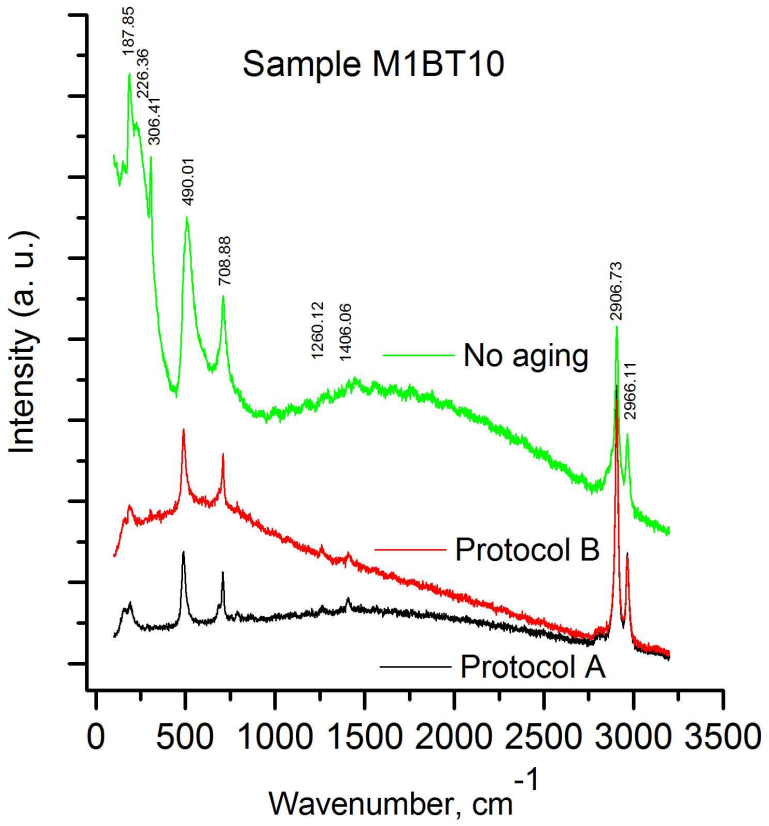

Figure 4S. Comparative Raman spectra of the sample M1BT10, original and aging by protocols A and B.

Table 1S. The main values of the diffractograms for the sample M2BT10 in the three stages as compared with those for barium titanate

BaO_3Ti		Sample M2BT10					
		No aged		Protocol A		Protocol B	
Angle, 2-Theta °	d value, Angstrom	Angle, 2-Theta °	d value, Angstrom	Angle, 2-Theta °	d value, Angstrom	Angle, 2-Theta °	d value, Angstrom
22.23	3.996	22.28	3.988	22.33	3.979	22.25	3.992
31.62	2.827	31.63	2.827	31.70	2.820	31.62	2.827
38.96	2.310	38.99	2.308	39.05	2.305	38.97	2.309
45.29	2.001	45.32	2.000	45.42	1.995	45.33	1.999
50.98	1.790	51.11	1.786	51.03	1.788	50.99	1.789
56.24	1.634	56.28	1.633	56.33	1.632	56.27	1.634
65.89	1.416	65.97	1.415	66.03	1.414	65.96	1.415

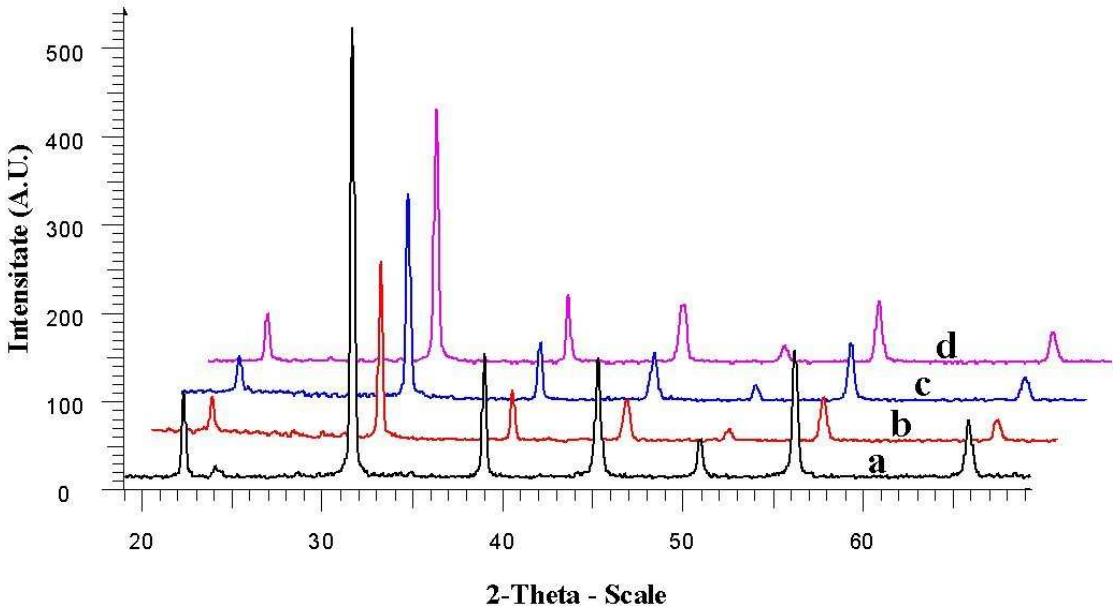

Figure 5S. WAXD patterns for: a-barium titanate as compared with sample M2BT15: b- no-aging; c-aged according to protocol A; d- aged according to protocol B.

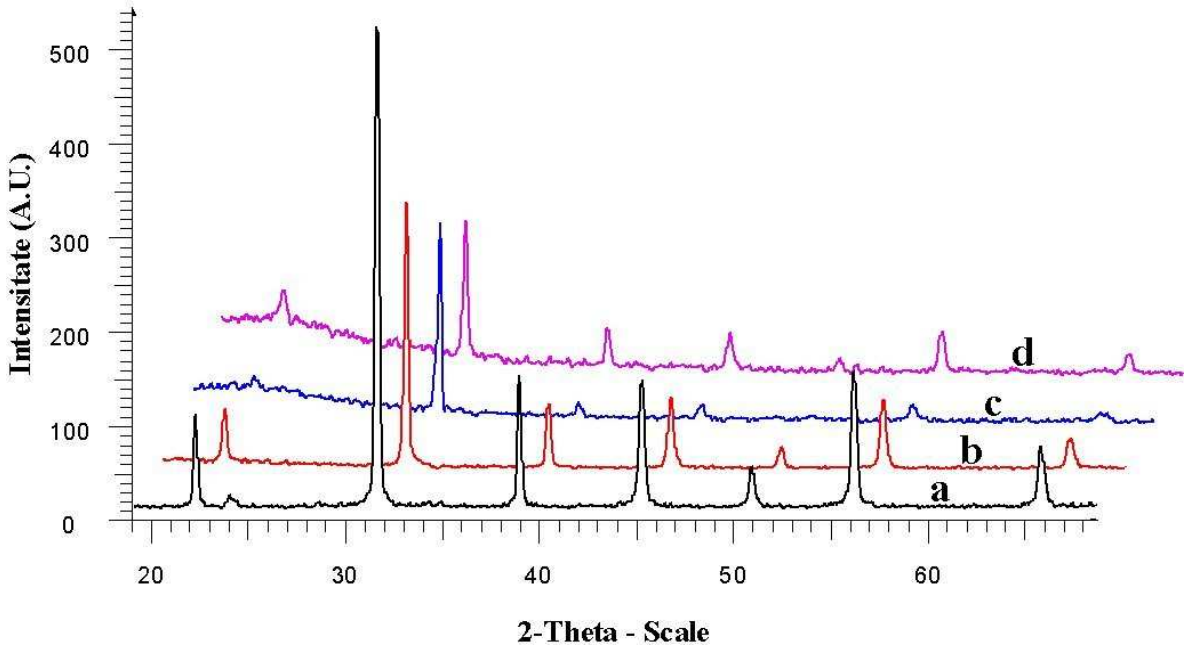

Figure 6S. WAXD patterns for: a-barium titanate as compared with sample M1BT10: b- no-aging; c-aged according to protocol A; d- aged according to protocol B.

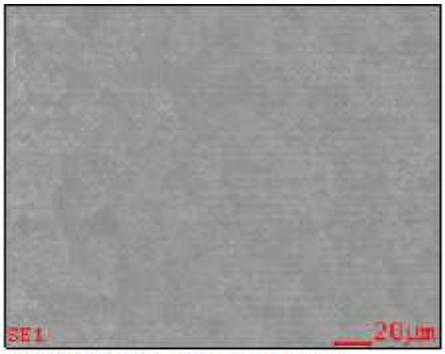

Element	Wt%	At%
CK	25.83	46.06
OK	21.02	28.14
NaK	02.08	01.93
SiK	17.89	13.64
ClK	02.16	01.30
BaL	17.01	02.65
TiK	14.03	06.27
Matrix	Correction	ZAF

M2BT15 surface, Protocol B ageing

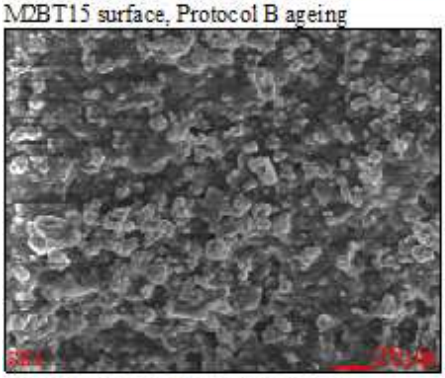

Element	Wt%	At%
CK	34.51	55.02
OK	17.25	20.65
NaK	02.23	01.86
SiK	22.78	15.53
ClK	03.26	01.76
SnL	00.70	00.11
BaL	10.11	01.41
TiK	09.15	03.66
Matrix	Correction	ZAF

M2BT15 section, Protocol B ageing

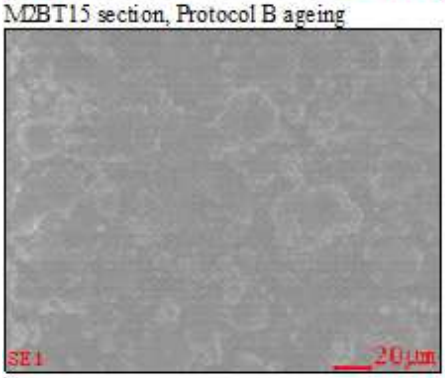

Element	Wt%	At%
CK	39.76	58.09
OK	18.88	20.71
NaK	02.88	02.19
SiK	23.07	14.41
ClK	03.39	01.68
BaL	06.29	00.80
TiK	05.74	02.10
Matrix	Correction	ZAF

M2BT15 surface, Protocol A ageing

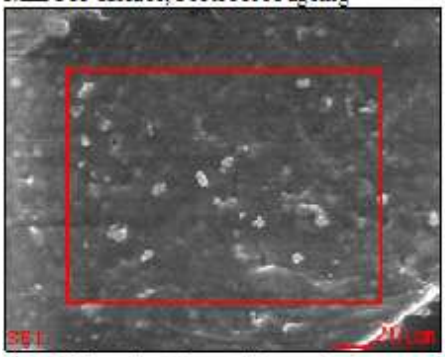

Element	Wt%	At%
CK	41.92	58.18
OK	19.05	19.84
NaK	00.15	00.11
SiK	35.37	20.99
ClK	00.27	00.13
SnL	00.37	00.05
BaL	01.31	00.16
TiK	01.57	00.55
Matrix	Correction	ZAF

M2BT15 section, Protocol A ageing

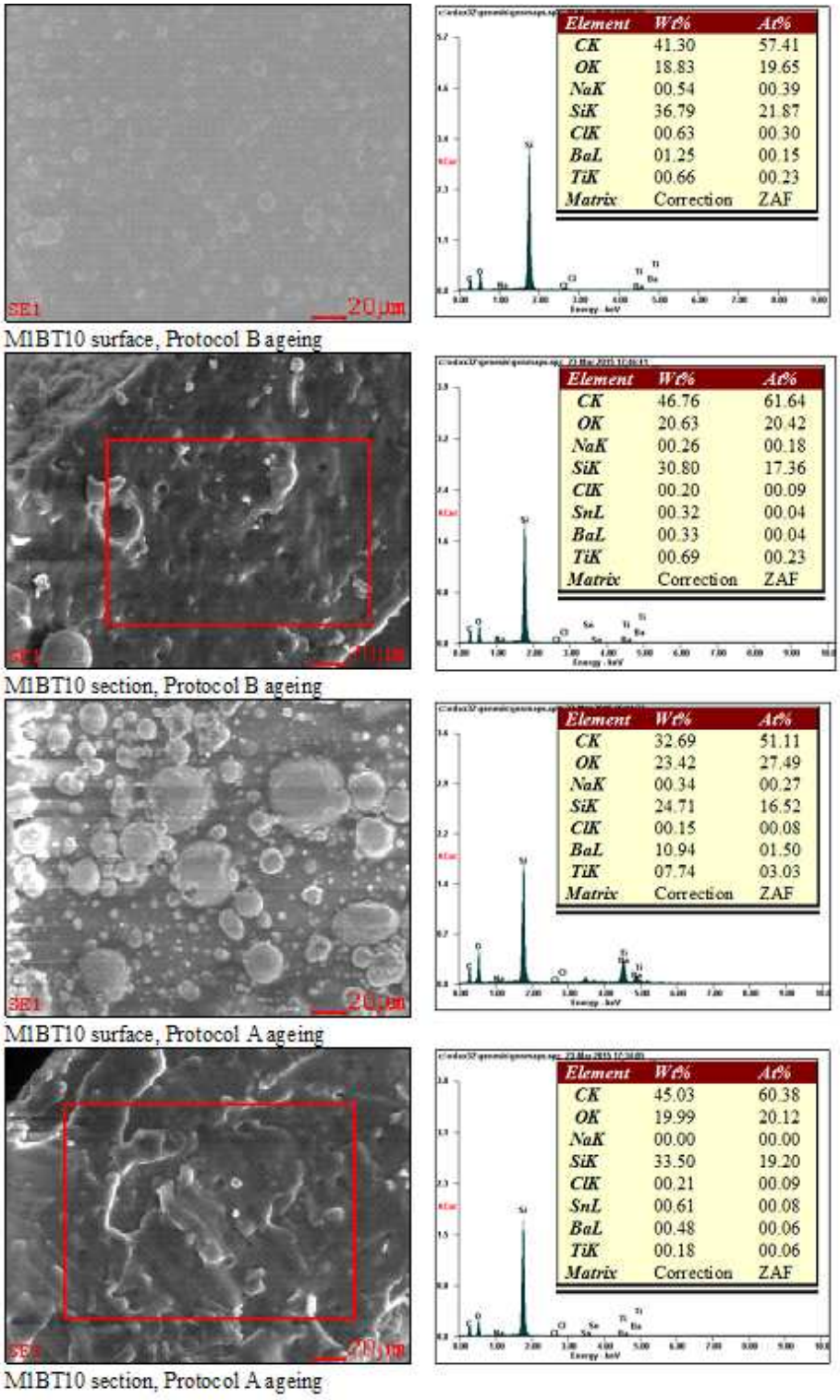

Figure 7S. EDX spectra and elemental content estimated for two of the samples, M2BT15 and M1BT10 aged by different protocols, on outer surface and in section.

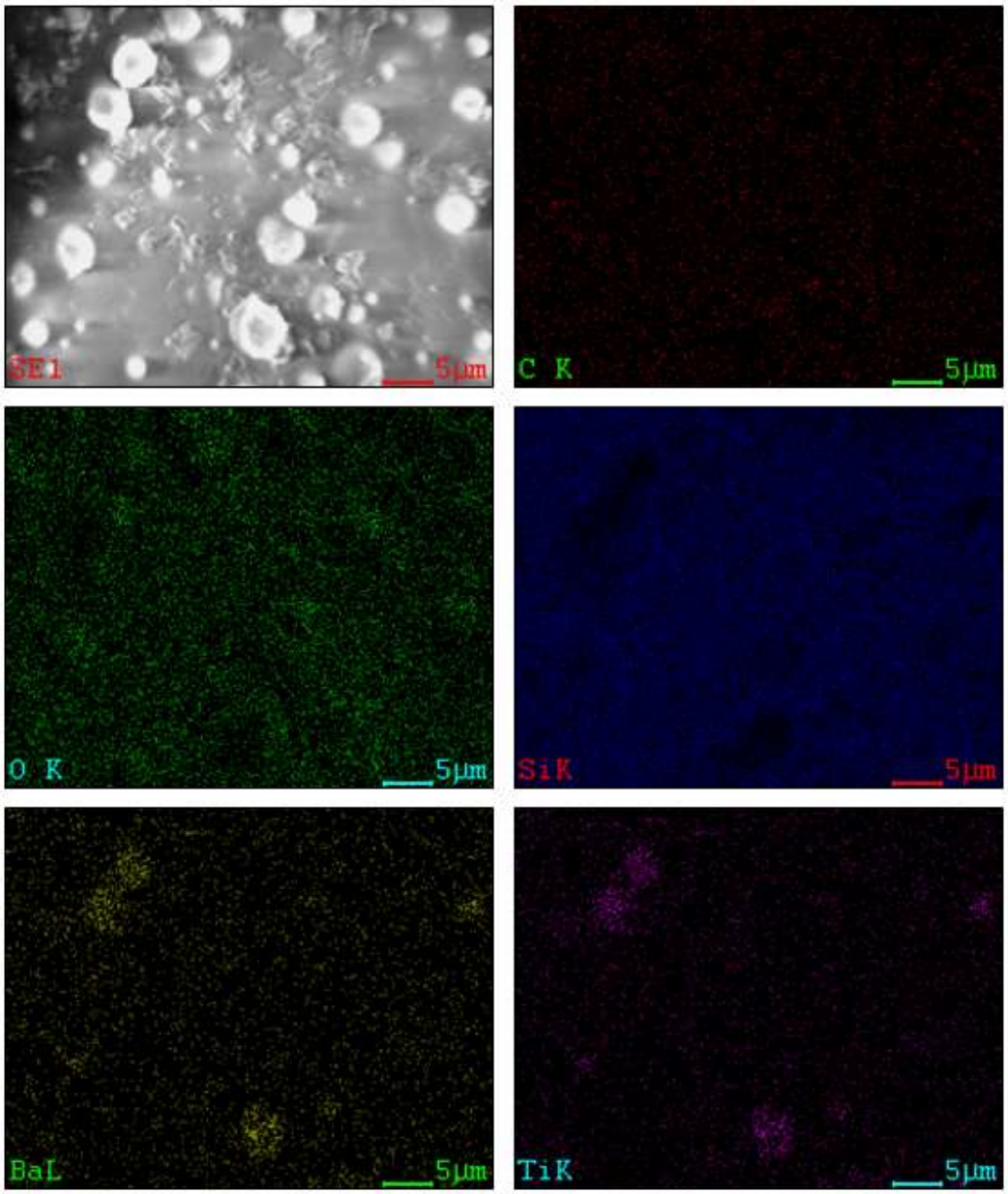

Figure 8S. Elements mapping on the surface of sample M1BT10 aged according to protocol A and subsequently washed with clean water.

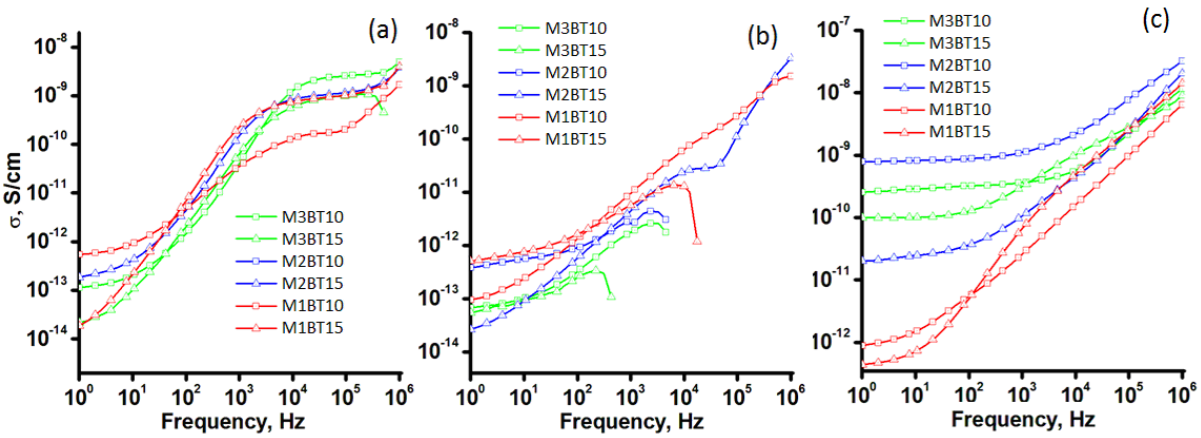

Figure 9S. Conductivity curves for the samples: left - no ageing; middle - after ageing according to protocol A; right - after ageing according to protocol B.

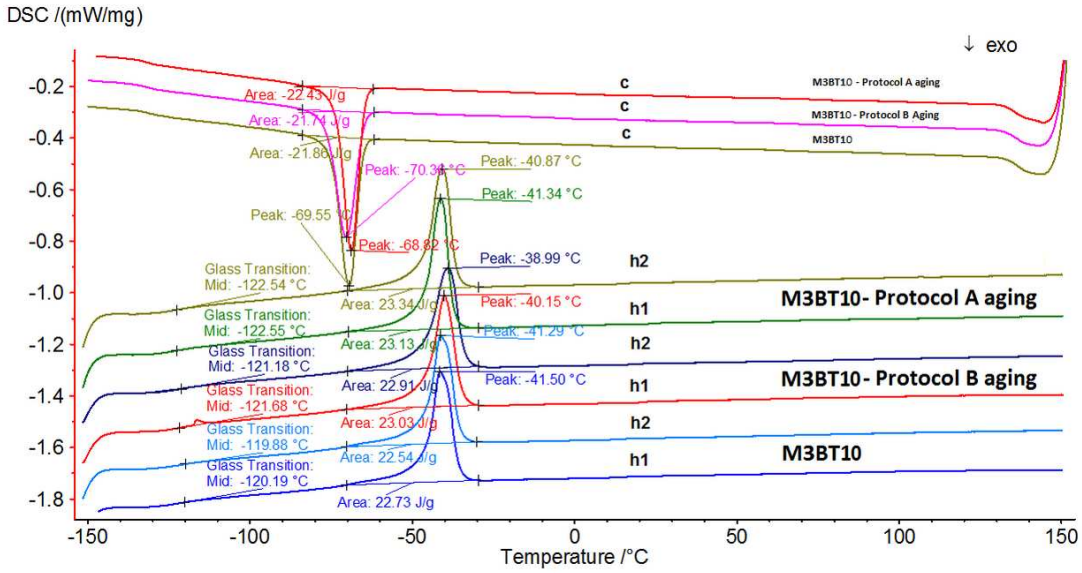
DSC /(mW/mg)
↓ exo
M3BT10 - Protocol A aging
M3BT10 - Protocol B Aging
M3BT10
Area: -22.43 J/g
Area: -21.74 J/g
Area: -21.86 J/g
Peak: -70.34 °C
Peak: -40.87 °C
Peak: -41.34 °C
Peak: -69.55 °C
Peak: -68.82 °C
Peak: -38.99 °C
Peak: -40.15 °C
Peak: -41.29 °C
Peak: -41.50 °C
Glass Transition: Mid: -122.54 °C
Glass Transition: Mid: -122.55 °C
Glass Transition: Mid: -121.18 °C
Glass Transition: Mid: -121.68 °C
Glass Transition: Mid: -119.88 °C
Glass Transition: Mid: -120.19 °C
Area: 23.34 J/g
Area: 23.13 J/g
Area: 22.91 J/g
Area: 23.03 J/g
Area: 22.54 J/g
Area: 22.73 J/g
c
h2
h1
M3BT10- Protocol A aging
M3BT10- Protocol B aging
M3BT10
-0.2
-0.4
-0.6
-0.8
-1.0
-1.2
-1.4
-1.6
-1.8
-150
-100
-50
0
50
100
150
Temperature /°C

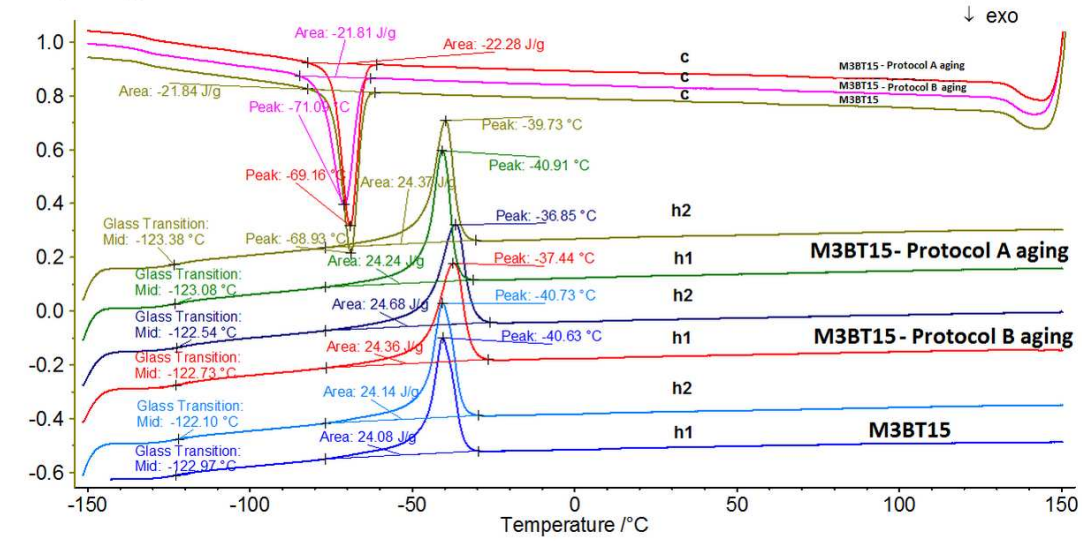
DSC /(mW/mg)
↓ exo
M3BT15 - Protocol A aging
M3BT15 - Protocol B aging
M3BT15
Area: -21.81 J/g
Area: -22.28 J/g
Area: -21.84 J/g
Peak: -71.05 °C
Peak: -39.73 °C
Peak: -40.91 °C
Peak: -69.16 °C
Area: 24.37 J/g
Peak: -36.85 °C
Peak: -68.93 °C
Peak: -37.44 °C
Peak: -40.73 °C
Peak: -40.63 °C
Glass Transition: Mid: -123.38 °C
Glass Transition: Mid: -123.08 °C
Glass Transition: Mid: -122.54 °C
Glass Transition: Mid: -122.73 °C
Glass Transition: Mid: -122.10 °C
Glass Transition: Mid: -122.97 °C
Area: 24.24 J/g
Area: 24.68 J/g
Area: 24.36 J/g
Area: 24.14 J/g
Area: 24.08 J/g
c
h2
h1
M3BT15- Protocol A aging
M3BT15 - Protocol B aging
M3BT15
1.0
0.8
0.6
0.4
0.2
0.0
-0.2
-0.4
-0.6
-150
-100
-50
0
50
100
150
Temperature /°C

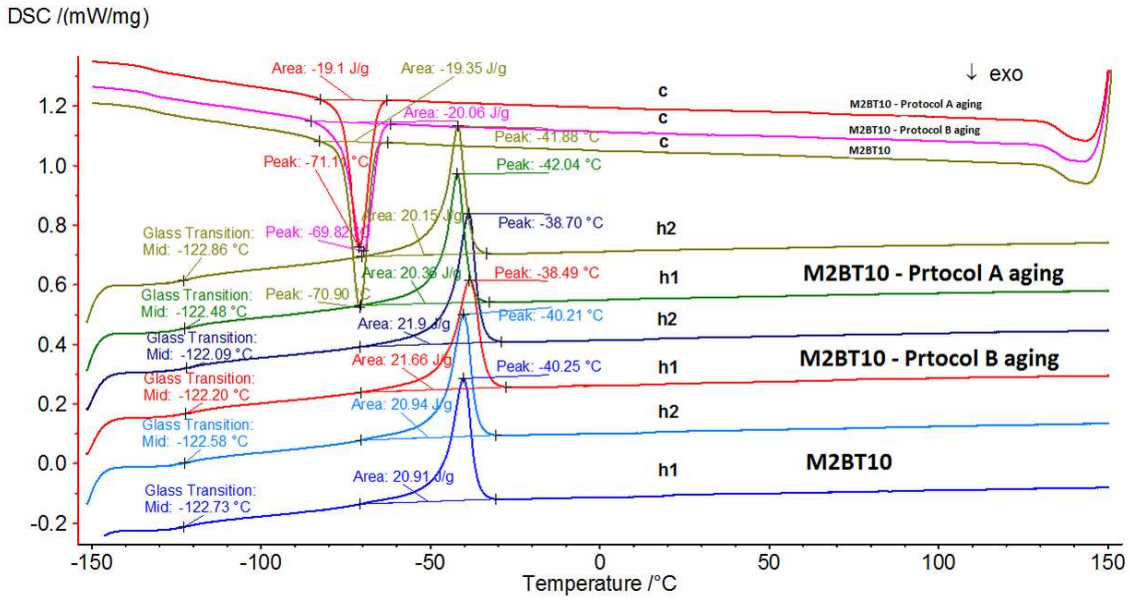
DSC /(mW/mg)
↓ exo
Area: -19.1 J/g
Area: -19.35 J/g
Area: -20.06 J/g
Peak: -71.11 °C
Peak: -41.88 °C
Peak: -42.04 °C
Peak: -38.70 °C
Peak: -38.49 °C
Peak: -40.21 °C
Peak: -40.25 °C
Area: 20.15 J/g
Area: 20.36 J/g
Area: 21.9 J/g
Area: 21.66 J/g
Area: 20.94 J/g
Area: 20.91 J/g
Glass Transition: Mid: -122.86 °C
Glass Transition: Mid: -122.48 °C
Glass Transition: Mid: -122.09 °C
Glass Transition: Mid: -122.20 °C
Glass Transition: Mid: -122.58 °C
Glass Transition: Mid: -122.73 °C
c
c
c
h2
h1
h2
h1
h2
h1
M2BT10 - Protocol A aging
M2BT10 - Protocol B aging
M2BT10
M2BT10 - Prtocol A aging
M2BT10 - Prtocol B aging
M2BT10
1.2
1.0
0.8
0.6
0.4
0.2
0.0
-0.2
-150
-100
-50
0
50
100
150
Temperature /°C

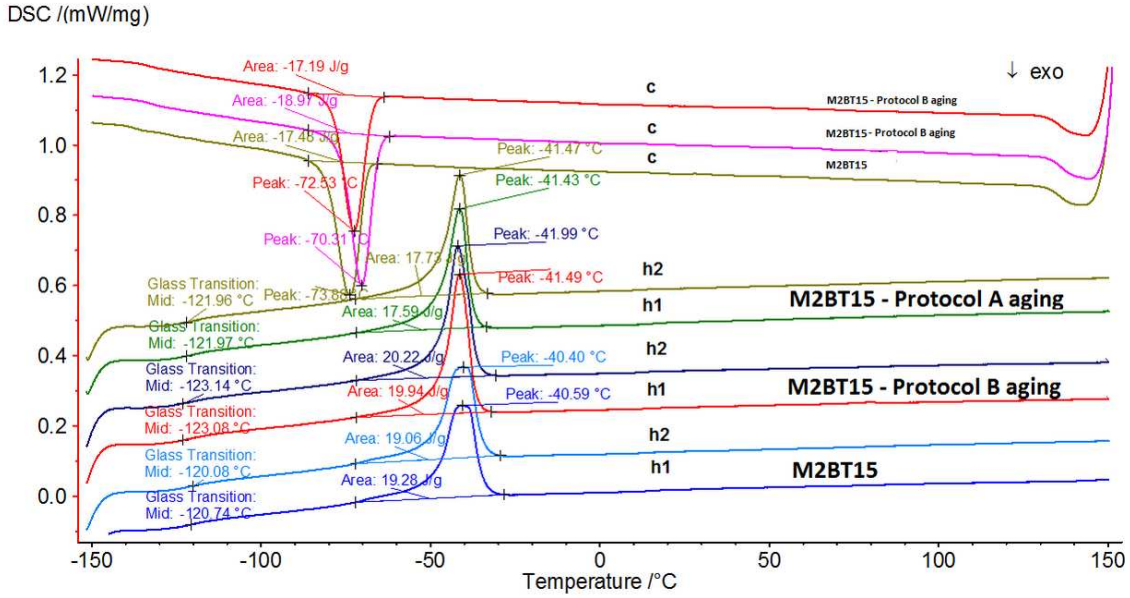
DSC /(mW/mg)
↓ exo
Area: -17.19 J/g
Area: -18.97 J/g
Area: -17.48 J/g
Peak: -72.53 °C
Peak: -70.31 °C
Peak: -41.47 °C
Peak: -41.43 °C
Peak: -41.99 °C
Peak: -41.49 °C
Peak: -40.40 °C
Peak: -40.59 °C
Area: 17.73 J/g
Area: 17.59 J/g
Area: 20.22 J/g
Area: 19.94 J/g
Area: 19.06 J/g
Area: 19.28 J/g
Glass Transition: Mid: -121.96 °C
Glass Transition: Mid: -121.97 °C
Glass Transition: Mid: -123.14 °C
Glass Transition: Mid: -123.08 °C
Glass Transition: Mid: -120.08 °C
Glass Transition: Mid: -120.74 °C
c
c
c
h2
h1
h2
h1
h2
h1
M2BT15 - Protocol B aging
M2BT15- Protocol B aging
M2BT15
M2BT15 - Protocol A aging
M2BT15 - Protocol B aging
M2BT15
1.2
1.0
0.8
0.6
0.4
0.2
0.0
-150
-100
-50
0
50
100
150
Temperature /°C

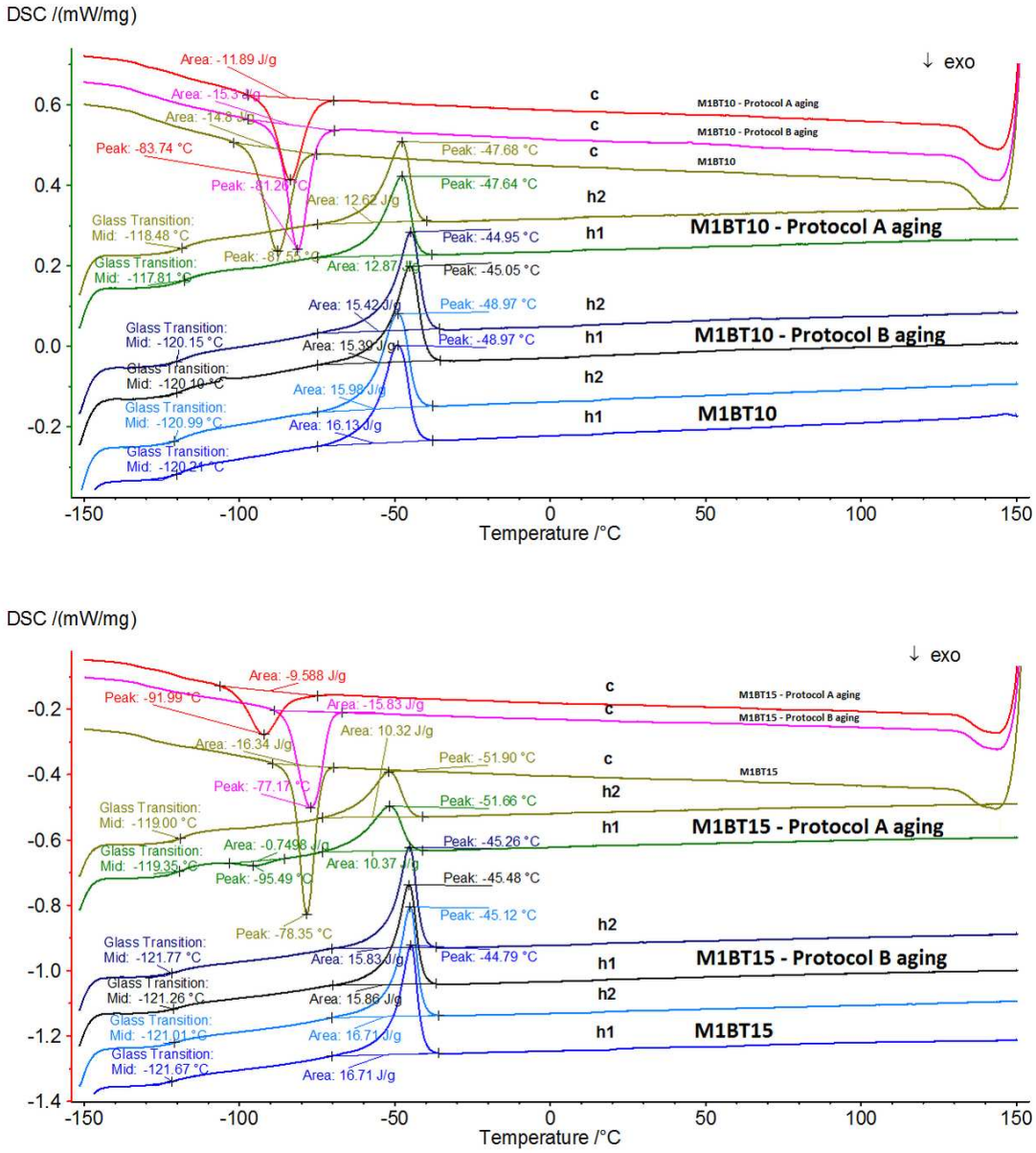

Figure 10S. DSC curves for all samples in different aging stages.